Investigation of various wall modeling approaches for LES in the presence of mild pressure gradients

***O. Thiry*[1]*, M. Duponcheel*[1] *and G. Winckelmans*[1]**

[1] ***Institute of Mechanics, Materials and Civil Engineering (iMMC), Université catholique de Louvain (UCL), 1348 Louvain-la-Neuve, Belgium***

olivier.thiry@uclouvain.be

Abstract

This work focuses on the investigation of various wall modeling strategies for the large-eddy simulation (LES) of high Reynolds number wall-bounded turbulent flows with mild pressure gradients. A half channel flow setup at $Re_\tau = 2000$ is considered. A periodic blowing and suction at the upper boundary is added to obtain a fluctuating pressure gradient. A wall-resolved LES is first performed to provide a reference solution and insight into the flow topology. Wall-modeled LES is then considered. Two strategies are investigated and compared. First, algebraic models are considered, without and with pressure gradient correction to the law of the wall used by the model. We also investigate various spatial and temporal averaging techniques when using the model. Second, RANS sub-layer models are considered, without and with pressure gradient corrections to the turbulent eddy viscosity model.

1 Introduction

The present work focuses on analysing the behavior of various wall modeling strategies for LES in the presence of mild pressure gradients. The case we here consider is represented in Fig. 1. It is a "half channel flow" set-up, with no slip at the bottom ($y = 0$), and slip with blowing and suction at the top ($y = h$) in order to generate the desired acceleration-deceleration profile. The flow is periodic in the streamwise (x) and spanwise (z) directions, and the computational domain size is $L_x \times L_y \times L_z = 4\pi h \times h \times \pi h$. At $y = h$, we impose:

$$\frac{\partial u}{\partial y} = \frac{\partial w}{\partial y} = 0 \tag{1}$$

$$v(x, h, z) = v_{max} \sin\left(2\pi \frac{x}{L_x}\right) . \tag{2}$$

The incompressible Navier-Stokes equations are solved with the addition of a mean pressure gradient forcing term $-\left(\frac{dP}{dx}\right)_F = u_{\tau,F}^2$, and in the context of LES, hence with a subgrid scales (SGS) stress tensor, $\sigma_{ij}^{sgs} = \tau_{ij}^{sgs} + \frac{1}{3}\sigma_{kk}^{sgs}\delta_{ij}$. We here only model the deviatoric part of the SGS tensor, the trace being incorporated into the effective reduced pressure, $P = \frac{p}{\rho} - \frac{1}{3}\sigma_{kk}^{sgs}$:

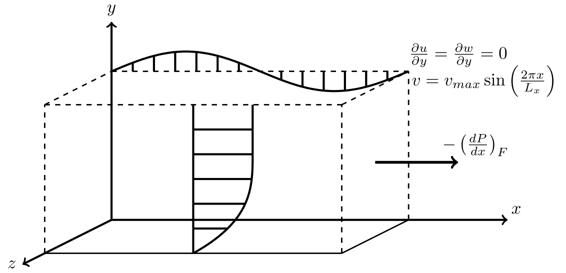

Figure 1: Channel flow setup with blowing and suction at the top of the computational domain.

$$\frac{\partial u_j}{\partial x_j} = 0 \tag{3}$$

$$\frac{\partial u_i}{\partial t} + \frac{\partial}{\partial x_j}(u_i u_j) = -\left(\frac{dP}{dx_i}\right)_F - \frac{\partial P}{\partial x_i} + \frac{\partial}{\partial x_j}\left(2\nu S_{ij} + \tau_{ij}^{sgs}\right) . \tag{4}$$

We use a regularized multiscale SGS model with the WALE scaling, as described in Bricteux et al. (2009), in its small-all form, see Cocle et al. (2009). Hence, the small scales are here used to compute the SGS viscosity only. The forcing pressure gradient is used to perform the global non-dimensionalisations: $u^* = \frac{u}{u_{\tau,F}}$ and $y^* = \frac{y\, u_{\tau,F}}{\nu}$. The global Reynolds number is defined as $Re_{\tau,F} = \frac{u_{\tau,F}\, h}{\nu} = 2000$. The blowing intensity is set to $v_{max} = 1.25\, u_{\tau,F}$, corresponding to a blowing flow rate $Q = \int_0^{L_x/2} v(x,h)\, dx = 5\, u_{\tau,F}\, h$. The strength of the local pressure gradient is characterized using either p^+ or the pressure velocity u_p : $p^+ = \frac{\nu}{u_\tau^3}\frac{dP}{dx} = \frac{u_p^3}{u_\tau^3}$, where the mean forcing pressure gradient is of course not accounted for. The equations are solved numerically using a fourth order finite difference code that conserves momentum exactly, and conserves energy up to fourth order. A wall-resolved LES (WRLES) is first performed to obtain a reference solution, using a $N_x \times N_y \times N_z = 640 \times 192 \times 256$

mesh and with a hyperbolic tangent stretching in the y direction:

$$\frac{y}{h} = 1 + \frac{\tanh(\gamma\,(\xi - 1))}{\tanh(\gamma)} \ , \qquad (5)$$

with $\gamma = 2.75$, and $\xi \in [0;1]$. This results in cells of size $\Delta x^* = 39$, $\Delta y^* = 0.5 - 28$ and $\Delta z^* = 24$. Here, we distinguish y^* defined using the global friction velocity $u_{\tau,F}$ from $y^+ = \frac{y\,u_\tau}{\nu}$ defined using the local friction velocity:

$$u_\tau = \left(\frac{|\overline{\tau_{\mathbf{w}}}|}{\rho} \right)^{\frac{1}{2}} , \qquad (6)$$

where $\overline{\cdot}$ stands for averaging over span and time. Since the actual u_τ does not exceed $1.1\,u_{\tau,F}$, see later in Fig. 6, these cell sizes lie well within the bounds proposed by Sagaut (2006) for WRLES. The simulation was run for a total time $T\,\overline{u}_{bulk,min}/L_x = 92$, and the statistical averaging started at $t\,\overline{u}_{bulk,min}/L_x = 55$.

Flow topology

The flow is periodically accelerated and decelerated by the imposed vertical velocity profile at the top, of Eq. (2). We see, in Fig. 6, that the wall response is not in phase with the vertical velocity profile, and that the minimum wall shear stress is reached before $x/L_x = 0.50$. The wall friction first decreases due to the flow deceleration, then increases due to flow acceleration, but the wall friction minimum is reached before the center of the numerical box. This is also visible in Fig. 2, where a snapshot of instantaneous wall friction is displayed. Fig. 2 also displays the signature of the turbulent structures close to the wall. Long streaks are seen in the accelerated part of the flow, while these structures are broken down to more streamwise incoherent structures in the decelerated part of the flow. This is consistent with the observations of Na and Moin (1998).

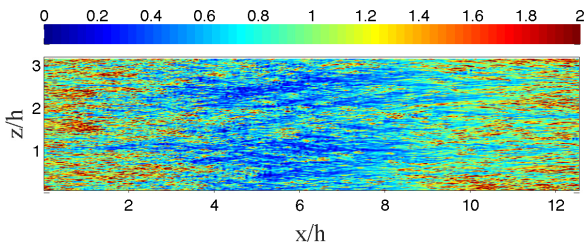

Figure 2: Instantaneous wall friction $\tau^*_{w,x}$.

The mean flow streamlines are shown in Fig 3 along with mean velocity profiles at a few streamwise stations. The acceleration/deceleration of the flow through blowing and suction is visible through the broadening of the streamlines at the channel center, corresponding to the lowest mass flow rate. Another feature of the flow is the existence of a mean *dividing streamline* above which the flow is essentially laminar. Downstream of $x/L_x = 0.5$, a "laminar shower" is blown into the flow, some of which will be sucked back in the suction part of the flow. Most of the flow turbulence is contained below the dividing streamline, as can be seen in Fig. 4 as $x/L_x = 0$. Turbulent structures are lifted from the wall between $x/L_x = 0$ and 0.5 and blown towards the wall between $x/L_x = 0.5$ and 1.

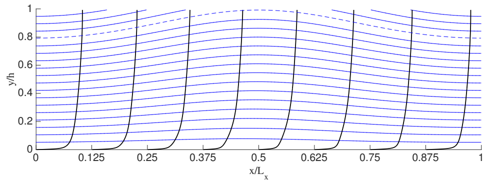

Figure 3: Mean streamlines (thin solid; the dividing streamline being dashed) and velocity profiles (thick solid).

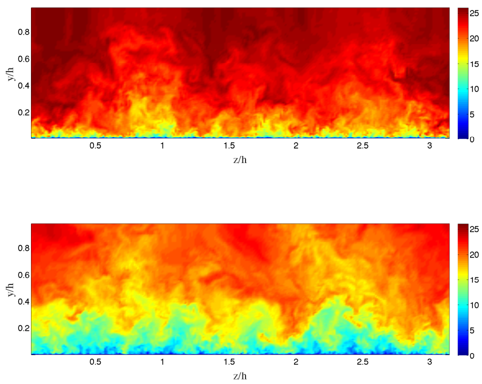

Figure 4: Instantaneous streamwise velocity $u/u_{\tau,F}$ at $x/L_x = 0$ (top) and 0.5 (bottom).

2 Assessment of various wall modeling strategies

Wall-modeled LES is then considered, using a coarse $128 \times 32 \times 48$ and uniform mesh. This mesh has a viscous resolution of $\Delta x^* = 196$, $\Delta y^* = 62.5$, and $\Delta z^* = 130$. Two strategies are investigated: algebraic wall models and RANS sub-layer models, based on the turbulent boundary layer (TBL) equations and turbulent eddy viscosity RANS models.

Algebraic wall models

When considering algebraic wall models, several issues arise: from a law of the wall (LOTW) that is considered valid in the mean, compute a mean friction velocity and, from that, compute a local wall shear stress. Local and averaged flow information is therefore required. The developments are based on a generic local averaging procedure $\langle\cdot\rangle$. Averaging strategies are discussed later on. From a chosen LOTW, $u^+ = f(y^+)$, and for a given averaged velocity $\langle \mathbf{u} \rangle$, the mean friction velocity u_τ can be obtained by solving the nonlinear equation:

$$|\langle \mathbf{u} \rangle| - u_\tau\, f\left(\frac{y\, u_\tau}{\nu}\right) = 0\ , \qquad (7)$$

as suggested by Grötzbach (1987). The first LOTW we consider is that of Reichardt (1951):

$$u^+ = \frac{1}{\kappa}\log\left(1+\kappa y^+\right) + \left(B - \frac{1}{\kappa}\log\left(\kappa\right)\right) \qquad (8)$$
$$\left(1-\exp\left(-\frac{y^+}{11}\right) - \frac{y^+}{11}\exp\left(-0.33y^+\right)\right)\ ,$$

hence only accounting for mean wall friction, independently of pressure gradient effects. This law is equivalent to the log law in the log layer, and connects it smoothly with the viscous sub-layer. It is more accurate than the law of Spalding (1961), and it also exhibits better convergence properties when solving Eq. (7).

Once a mean friction velocity is obtained, one must compute a local wall shear stress $\tau_\mathbf{w}$. One approach, similar to that of Schumann (1975), consists in imposing the wall shear stress in the direction of the local velocity and with an intensity proportional to the velocity with respect to its local average:

$$\tau_\mathbf{w} = \rho \frac{\mathbf{u}}{|\langle \mathbf{u} \rangle|} u_\tau^2\ . \qquad (9)$$

The same principle can be applied quadratically (as done by Khanna and Brasseur (1997)). The wall shear stress is then computed in the direction of the local velocity but the amplitude is computed based on the square of the velocity:

$$\tau_\mathbf{w} = \rho \frac{\mathbf{u}\,|\mathbf{u}|}{|\langle \mathbf{u}\,|\mathbf{u}|\rangle|} u_\tau^2\ . \qquad (10)$$

The model of Eq. (10) can be seen as modeling the inner layer of the TBL using a drag coefficient C_D. The wall shear stress then reads $\tau_\mathbf{w} = \frac{1}{2}\rho C_D\,|\mathbf{u}|\,\mathbf{u}$, where the drag coefficient is obtained from mean information:

$$C_D = \frac{2u_\tau^2}{|\langle \mathbf{u}\,|\mathbf{u}|\rangle|}\ . \qquad (11)$$

When a pressure correction is applied, the same procedure can be used, with a slight modification. Shih et al. (1999) proposed a wall model based on a modified LOTW to account for both wall friction and pressure gradient. The model they propose identifies two separate contributions to the velocity field:

$$\mathbf{u} = u_\tau\, f_1\left(\frac{y u_\tau}{\nu}\right)\hat{\mathbf{n}}_\tau + u_p\, f_2\left(\frac{y u_p}{\nu}\right)\hat{\mathbf{n}}_\mathbf{p} = \mathbf{u_1} + \mathbf{u_2}\ , \qquad (12)$$

where $\hat{\mathbf{n}}_\tau$ and $\hat{\mathbf{n}}_\mathbf{p}$ are unit vectors in the direction of the wall shear stress and of the pressure gradient, respectively. They used Spalding's LOTW for f_1 and proposed a piecewise representation of f_2. Here, we use Reichardt's LOTW for f_1 and the original f_2, with adjusted coefficients so as to obtain a continuous function. The methodology is as follows. First, the locally averaged pressure gradient $\langle \nabla P \rangle$ is computed, as well as $u_p = \left(\nu\,\langle \nabla P \rangle\right)^{1/3}$. From this, $\mathbf{u_2}$ is obtained:

$$\mathbf{u_2} = u_p\, f_2\left(\frac{y\, u_p}{\nu}\right)\frac{\langle \nabla P \rangle}{|\langle \nabla P \rangle|}\ , \qquad (13)$$

and the velocity $\mathbf{u_1} = \mathbf{u} - \mathbf{u_2}$ is computed. The *pressure corrected* velocity $\mathbf{u_1}$ is then used to obtain u_τ from $|\langle \mathbf{u_1} \rangle| = u_\tau\, f_1\left(\frac{y\, u_\tau}{\nu}\right)$. The local wall shear stress can then be computed by substituting u_τ and $\mathbf{u_1}$ either in Eq. (9) or in Eq. (10).

Various local averaging techniques are used and compared: averaging over the homogeneous spanwise direction z, local averaging over the n_x and n_z closest neighbors, and averaging over time. The directions over which the averaging is performed must be homogeneous or sufficiently slowly varying with respect to the grid size in that direction of space. In the present case, this is true in the spanwise and streamwise directions. The local averaging procedure is then defined by n_x and n_z. The time averaging is performed using an exponential filtering strategy, so as to avoid having to keep a large amount of data for the averaging procedure. The filter is as follows:

$$\big\langle u \big\rangle(t+\Delta t) = (1-c_{\exp})\,\big\langle u \big\rangle(t) + c_{\exp}\, u(t+\Delta t)\ , \qquad (14)$$

with $0 < c_{\exp} \leq 1$. The closer $c_{\exp}$ is to zero, the more the averaging. The coefficient $c_{\exp}$ is tied to the cutoff frequency of the exponential filter f_c at which the modal amplitude is halved. Cahuzac et al. (2010) showed that assuming $f_c \Delta t \ll 1$ we get:

$$c_{\exp} \simeq 3.63\, f_c\, \Delta t\ . \qquad (15)$$

The information fed to the wall models does not need to come from the first layer of points: it can be chosen at any point in the log layer or below. Kawai and Larsson (2012) showed that it is required to take the information further from the wall than the first layer of points. This is due to the fact that large SGS modeling errors and numerical errors affect the first layers, closest to the wall. We here used the third layer of points to get the flow information.

RANS sub-layer models

RANS sub-layer models are then considered. The turbulent boundary layer (TBL) equations are solved, similarly to Balaras et al. (1996). The RANS mesh is embedded within the first few wall cells. The upper boundary condition for the RANS is provided by the LES field at the third off-wall point and the mesh is such that the RANS is wall-resolved: it has 15 points in the y direction, with a hyperbolic tangent stretching (see Eq. (5)) with $\gamma = 2.7$. The generic TBL equations read:

$$\frac{\partial u_i}{\partial t} + \frac{\partial}{\partial x_j}(u_i u_j) = -\left(\frac{\partial P}{\partial x_i}\right)_F - \frac{\partial P}{\partial x_i} + \frac{\partial}{\partial x_j}\Big(2(\nu+\nu_t)S_{ij}\Big), \qquad i = 1,3 \quad (16)$$

$$u_2 = -\int_0^{x_2}\left(\frac{\partial u_1}{\partial x_1} + \frac{\partial u_3}{\partial x_3}\right)dx_2', \quad \frac{\partial P}{\partial x_2} = 0 \quad (17)$$

We here solve all terms of the equations, including the time derivative, the convective terms and the pressure term. At the wall, the no-slip boundary condition is imposed. At the top, the LES field provides the velocity boundary condition and the pressure gradient. The velocity field of the LES contains many fluctuations, and some local averaging is performed to damp the smallest scales of the LES when feeding it to the RANS. The resulting velocity field still contains some resolved fluctuations, whereas the ideal RANS solution is in the present case stationary. To avoid accounting for those resolved fluctuations twice (in the RANS term and in the convective term), we use the correction proposed by Medic et al. (2005):

$$\nu_{t,corr} = \nu_t + \frac{\langle u'v'\rangle}{\frac{du}{dy}}, \quad (18)$$

where ν_t is the value computed using the model and $\nu_{t,corr}$ is the corrected value used in the RANS equations. This approach is also close to (though less general than) that proposed by Park and Moin (2014).
Here, the effort is put on the investigation of various models for the turbulent eddy viscosity ν_t. The baseline is the model used (among others) by Cabot (1995), which is of the Van Driest (1956) damping type :

$$\nu_t = \kappa\, y\, u_\tau \left(1 - e^{-y^+/A^+}\right)^2, \quad (19)$$

where we here use $A^+ = 16$, and $\kappa = 0.38$. This model has the proper y^3 behavior near the wall and is therefore preferred to the model used by Balaras et al. (1996): $\nu_t = (\kappa y)^2|\mathbf{S}|\left(1 - e^{-(y^+/A^+)^3}\right)$, which has a y^5 behavior near the wall. The equations (16) already contain a pressure gradient term, but further corrections can be included in the turbulent eddy viscosity model itself. Two such models are investigated. The first is the model used by Duprat et al. (2011) (and based on the work of Nituch et al. (1978)):

$$\nu_t = \kappa\, y\, u_{\tau,p}\left(\alpha + y^{\tau,p}(1-\alpha)^{3/2}\right)^\beta \cdot\left(1 - \exp\left(\frac{y^{\tau,p}}{1+A\alpha^3}\right)\right)^2, \quad (20)$$

with $u_{\tau,p} = \sqrt{u_\tau^2 + u_p^2}$, $\alpha = u_\tau^2/u_{\tau,p}^2$, and $y^{\tau,p} = y\, u_{\tau,p}/\nu$. We here used $\kappa = 0.38$, $\beta = 0.78$, and $A = 17$. Again, the forcing pressure gradient is not taken into account while computing ν_t. The second is the model proposed by Granville (1990):

$$\nu_t = \kappa\, y\, u_\tau\left(1 + ap^+\right)\left(1 - e^{-\left(\frac{y^+\sqrt{1+bap^+}}{A^+}\right)^2}\right) \quad (21)$$

where we here used $\kappa = 0.38$, $a = 0.9$, $b = 14.5$ if $p^+ > 0$ and $b = 18.0$ if $p^+ < 0$, and $A^+ = 24$.

Test of the models in classical channel flow

The various approaches are first tested in a standard channel flow, thus without fluctuating pressure gradient, at $Re_\tau = 2000$, and against the DNS data of Hoyas and Jimenez (2006). Fig. 5 displays the results of the linear and quadratic algebraic models (for both the Reichardt's and the Shih et al.'s LOTW, using a 5×5 averaging window), as well as the RANS sub-layer models, with the viscosity used by Cabot, Duprat et al. and Granville. The models are all able to accurately predict the velocity profile, only the model of Cabot leads to a small underestimation of the mass flow rate. We also have a good qualitative agreement for the velocity fluctuations, despite an underprediction of the total turbulent kinetic energy. Since the algebraic models are insensitive to the fact that the law of the wall is applied with the linear or the quadratic approach, only the quadratic approach will be used in what follows.

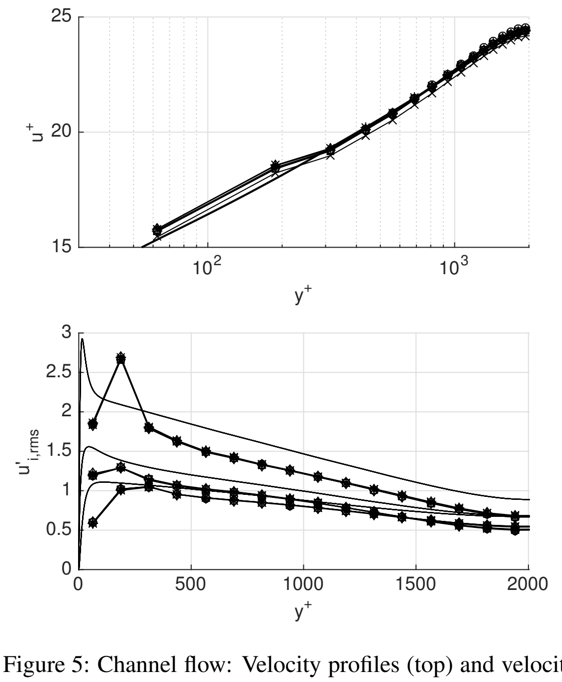

Figure 5: Channel flow: Velocity profiles (top) and velocity fluctuations (bottom). DNS of Hoyas and Jimenez (2006) (thick solid). Algebraic wall models: linear model with Reichardt's law (diamonds) and with Shih et al. law (squares); quadratic model with Reichardt's law (bullets) and with Shih et al. law (circles). RANS sublayers: Cabot (crosses), Duprat et al. (asterisks) and Granville (plusses).

3 Assessment of the models in the channel with blowing and suction

The friction velocity obtained using the wall models is shown and compared to the WRLES in Fig. 6. Reichardt's LOTW, with no pressure gradient correction, performs quite well on both the velocity profiles and the wall friction. We see that the model by Shih et al. here fails at predicting u_τ and exhibits a stronger reaction to the pressure gradient than the WRLES. We see, in Fig. 8, that it still recovers the mass flow rate rather well. Fig. 8 also shows the profiles computed using Shih et al.'s LOTW when using the values of u_τ and u_p as extracted from the WRLES (an *a priori* analysis). We see that the pressure gradient correction is too intense, hence the predicted profiles are overreacting to the pressure gradient. In the wall-modeled LES, the model therefore adapts its u_τ to recover the profiles, and hence fails at predicting u_τ. Variation of the averaging strategy did not change the results obtained using Reichardt's LOTW, as seen in Fig. 7; but time averaging slightly improved the wall friction predicted when using Shih et al.'s LOTW. The results still remained poor when compared to Reichardt's LOTW, as predicted by the a priori analysis.

All RANS sublayer models performed better than the under-resolved LES (i.e., no wall model) on both the velocity profiles and the wall friction. The results provided by the model of Cabot are the closest to the velocity profiles of the WRLES; but the three models tested here follow the trend of the WRLES rather well, despite an over- or under-estimation of the global mass flow rate. The wall friction obtained using the models of Duprat et al. and Granville are closer to the WRLES than that using the model of Cabot; hence showing that the pressure gradient corrections have in this case provided some improvement. None of the RANS sublayer models, however, provide results that are better than those obtained using the algebraic wall model with Reichardt's LOTW.

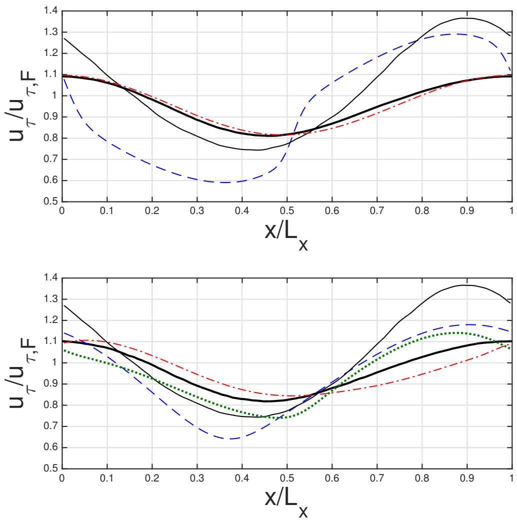

Figure 6: Friction velocity: WRLES (thick solid), no wall model (thin solid). Top: algebraic wall models; Reichardt's (dash-dot) and Shih et al.'s (dash). Bottom: RANS sub-layer wall models; Cabot (dash), Granville (dash-dot) and Duprat et al. (dot).

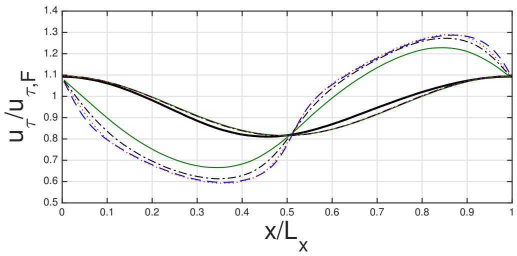

Figure 7: Friction velocity: algebraic wall models with Reichardt's and Shih et al.'s LOTW. Averaging over 5×5 points (dash), 3×3 points and $c_{\text{exp}} = 0.4$ (dash-dot), 1×25 points (dot), and $c_{\text{exp}} = 0.14$ (thin solid). The curves with Reichardt's LOTW are all superposed.

4 Conclusion

Wall-modeled LES had been investigated for a case with a mild pressure gradient, and using various strategies. Overall, it is unclear whether accounting for the pressure gradient in the wall models has provided improvement in this mild pressure gradient case. When the algebraic wall models were considered, the simplest model (i.e. using Reichardt's LOTW) was the best option, as it recovered fairly well both the velocity profiles and the wall friction. When RANS sublayer models were used, the additional pressure corrections included in the turbulent eddy viscosity model provided some improvement; yet none of the models could outperform the algebraic wall model using Reichardt's LOTW. In the presence of severe pressure gradients, and/or with separation of the boundary layer, pressure-corrected models could however prove of great importance.

Acknowledgments

Oliver Thiry is funded by a grant from Fond de la Recherche Scientifique de Belgique (F.R.S.-FNRS), Belgium. Computational resources have been provided by the supercomputing facilities of the Université catholique de Louvain (CISM/UCL) and the Consortium des Équipements de Calcul Intensif en Fédération Wallonie Bruxelles (CÉCI) funded by the F.R.S.-FNRS under convention 2.5020.11.

References

Balaras, E., Benocci, C., and Piomelli, U. (1996), Two-layer approximate boundary conditions for large-eddy simulations, *AIAA Journal*, 34(6).

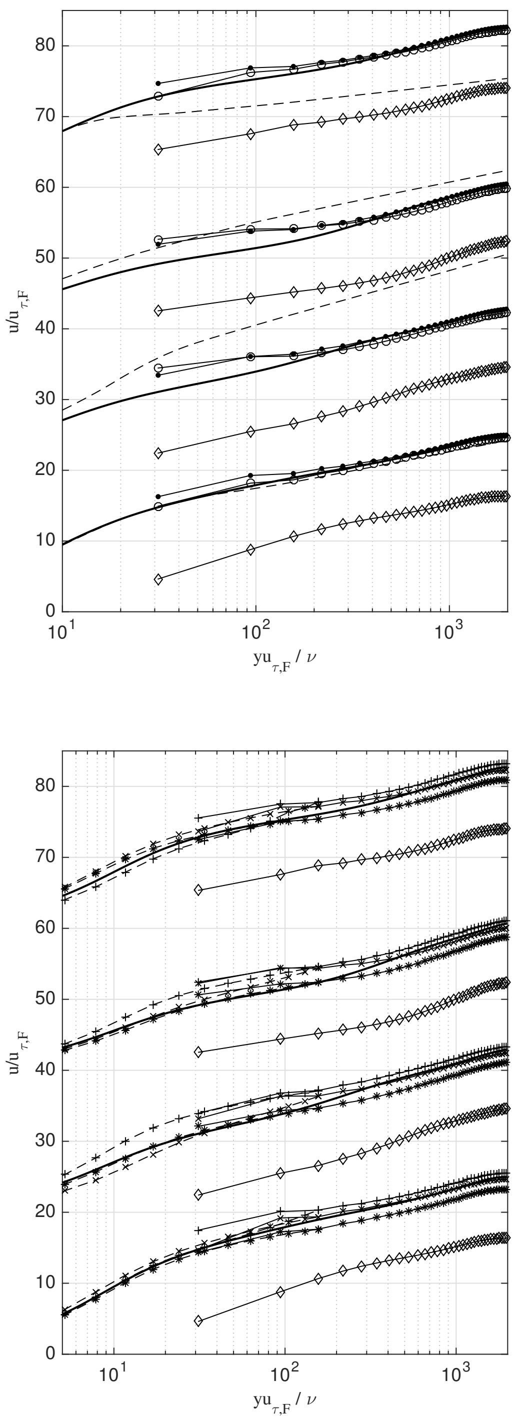

Figure 8: Velocity profiles a stations $x/L_x = 0$, 0.25, 0.50 and 0.75; each station being shifted upwards by 20 units for clarity. WRLES (thick solid), no wall model (diamonds). Top: algebraic wall models; Reichardt's (bullets), Shih et al.'s (circles), and Shih et al.'s in *a priori test* using values from the WRLES (thin dashed). Bottom: RANS sublayer models; Cabot (crosses), Duprat et al. (asterisks) and Granville (plusses).

Bricteux, L., Duponcheel, M., and Winckelmans, G. (2009), A multiscale subgrid model for both free vortex flows and wall-bounded flows, *Phys. Fluids*, 21(10):105102.

Cabot, W. (1995), Large-eddy simulation with wall models, *Annual Research Briefs, CTR*, pp. 41-50.

Cahuzac, A., Bouden, J., Borgnat, P., and Levêque, E. (2010), Smoothing algorithms for mean-flow extraction in large-eddy simulation of complex turbulent flows, *Phys. Fluids*, 22:125104.

Cocle, R., Bricteux, L., and Winckelmans, G. (2009), Scale dependence and asymptotic very high Reynolds number spectral behavior of multiscale subgrid models, *Phys. Fluids*, 21:085101.

Duprat, C., Balarac, G., Métais, O., Congedo, P. and Brugire, O. (2011), A wall-model for large-eddy simulations of turbulent flows with/out pressure gradient, *Phys. Fluids*, 23:015101.

Granville, P. S. (1990), A near-wall eddy viscosity formula for turbulent boundary layers in pressure gradients suitable for momentum, heat, or mass transfer, *J. Fluids Eng.*, 112:240-243.

Grötzbach, G. (1987), Direct numerical and large eddy simulation of turbulent channel flows, *Encyclopedia of Fluid Mechanics*, 6:1337-1391.

Hoyas, S. and Jimenez, J. (2006), Scaling of velocity fluctuations in turbulent channels up to $Re_\tau = 2000$, *Phys. Fluids*, 18:011702.

Kawai, S. and Larsson, J. (2012), Wall-modeling in large eddy simulation: length scales, grid resolution, and accuracy, *Phys. Fluids*, 24:015105.

Khanna, S. and Brasseur, J. G. (1997), Analysis of Monin-Obukhov similarity from large-eddy simulation, *J. Fluid Mech.*, 345:251-286.

Medic, G., Daeninck, G., Templeton, J., and Kalitzin, G. (2005), A frameworkfor near-wall RANS/LES coupling, *Annual Research Briefs, CTR*.

Na, Y. and Moin, P. (1998), Direct numerical dimulation of a separated tubrulent boundary layer, *J. Comput. Phys.*, 374:379-405.

Nituch, M. J., Sjolander, S. (1978), and M. R. Head, An improced version of the Cebeci-Smith eddy viscosity model, *Aeronaut. Q.*, 29:207-225.

Park, G. I. and Moin, P. (2014), An improved dynamic non-equilibrium wall-model for large eddy simulation, *Phys. Fluids*, 26(1):015108.

Reichardt, H. (1951), Vollständige darstellung der turbulenten geschwindigkeitverteilung in glatte leitungen (Complete representation of the turbulent velocity distribution in smooth pipes), *Zeitschrift fr Angewandte Mathematik und Mechanik (J. Appl. Math. and Mech.)*, 31(7):208-219.

Sagaut, P. (2006), Large-eddy simulation for incompressible flows: an introduction, Springer, 3rd edition.

Schumann, U. (1975), Subgrid scale model for finite differences simulations of turbulent flows in plane channels and annuli, *J. Comp. Phys.*, 18:376-404.

Shih, T.-H., Povinelli, L., Liu, N.-S., Potapczuk, M., and Lumley, J. L. (1999), A generalized wall function, Tech. report, NASA, Institute for Computational Mechanics in Propulsion.

Spalding, D. B. (1961), A single formula for the "law of the wall", *J. Appl. Mech.*, 28(3):455-458.

Van Driest, E. R. (1956), On turbulent flow near a wall, *J. Aeronaut. Sci.*, 23(11):1007-1011.